Stability analysis of snake robot locomotion based on averaging theory

Pål Liljebäck, Kristin Y. Pettersen, Øyvind Stavdahl, and Jan Tommy Gravdahl

***Abstract*— This paper investigates the controllability and stability properties of a planar snake robot influenced by anisotropic viscous ground friction. An analysis of the model shows that any asymptotically stabilizing control law for the robot to an equilibrium point must be *time-varying*. Furthermore, the analysis shows that the snake robot (with four links) is *strongly accessible* from *almost* any equilibrium point, except for certain singular configurations, and that the robot does *not* satisfy sufficient conditions for *small-time local controllability* (STLC). *Averaging theory* is employed to model the average velocity of the snake robot during *lateral undulation*. It is proven that the average velocity will converge exponentially fast to a steady state velocity, and an analytical expression for calculating the steady state velocity of the robot with an arbitrary number of links is presented. The paper presents simulation results that support the theoretical findings.**

I. Introduction

Inspired by biological snakes, snake robots carry the potential of meeting the growing need for robotic mobility in challenging environments. Snake robots consist of serially connected modules capable of bending in one or more planes. The many degrees of freedom of snake robots make them difficult to control, but provide traversability in irregular environments that surpasses the mobility of the more conventional wheeled, tracked and legged forms of robotic mobility. Research on snake robots has been conducted for several decades. However, our understanding of snake locomotion so far is for the most part based on empirical studies of biological snakes and simulation-based synthesis of relationships between parameters of the snake robot. This paper is an attempt to contribute to the understanding of snake robots by employing nonlinear system analysis tools for investigating fundamental properties of their dynamics.

There are several reported works aimed at analysing and understanding snake locomotion. Gray [1] conducted empirical and analytical studies of snake locomotion already in the 1940s. Hirose [2] studied biological snakes and developed mathematical relationships characterizing their motion, such as the *serpenoid curve*. Ostrowski [3] studied the controllability properties of a wheeled snake robot on a purely kinematic level. Saito *et al.* [4] optimized the parameters of the serpenoid curve based on simulations of a planar snake robot. Hicks [5] investigated general requirements for the propulsion of a three-linked snake robot. Nilsson [6] employed energy arguments to analyse planar snake locomotion with isotropic friction. Transeth *et al.* [7] proved that the velocity of a planar snake robot is bounded. Li *et al.* [8] studied the controllability of the joint motion of a snake robot. The authors have previously studied the stability properties of snake locomotion based on *Poincaré maps* and investigated the controllability properties of a planar snake robot influenced by anisotropic friction [9].

Research on robotic fish and eel-like mechanisms is relevant to research on snake robots since these mechanisms are very similar. The works in [10]–[12] investigate the controllability of various fish-like mechanisms, synthesize gaits for translational and rotational motion based on Lie bracket calculations, and propose controllers for tracking straight and curved trajectories.

The purpose of this paper is to investigate the controllability and stability properties of planar snake locomotion based on a simplified model recently proposed by the authors [13]. The paper has two contributions. The first contribution is an analysis that shows that any asymptotically stabilizing feedback control law for the snake robot to an equilibrium point must be *time-varying*. Furthermore, the analysis shows that the snake robot is *strongly accessible* from *almost* any equilibrium point, except for certain singular configurations, and that the robot does *not* satisfy sufficient conditions for *small-time local controllability* (STLC). The second contribution is the use of *averaging theory* to investigate the velocity dynamics of the snake robot during *lateral undulation*. The average velocity of the snake robot is shown to converge exponentially fast to a steady state velocity, and an analytical expression for calculating the steady state velocity is presented as a function of the various controller parameters. To the authors' best knowledge, this is the first published formal proof that a wheel-less snake robot with anisotropic ground friction properties achieves forward propulsion when it moves by lateral undulation. The paper presents simulation results that support the theoretical findings.

The paper is organized as follows. Section II presents the model of the snake robot. Section III investigates the stabilizability properties of the robot, while the controllability properties are investigated in Section IV. Section V presents a controller for lateral undulation. Section VI analyses the stability of the velocity dynamics based on averaging theory. Section VII presents simulation results. Finally, Section VIII presents concluding remarks.

II. The model of the snake robot

This section summarizes the simplified model of a planar snake robot which is described in detail in [13].

Affiliation of Pål Liljebäck is shared between the Department of Engineering Cybernetics at the Norwegian University of Science and Technology, NO-7491 Trondheim, Norway, and SINTEF ICT, Dept. of Applied Cybernetics, N-7465 Trondheim, Norway. E-mail: Pal.Liljeback@sintef.no

K. Y. Pettersen, Øyvind Stavdahl, and Jan Tommy Gravdahl are with the Department of Engineering Cybernetics at the Norwegian University of Science and Technology, NO-7491 Trondheim, Norway. E-mail: {Kristin.Y.Pettersen, Oyvind.Stavdahl, Tommy.Gravdahl}@itk.ntnu.no

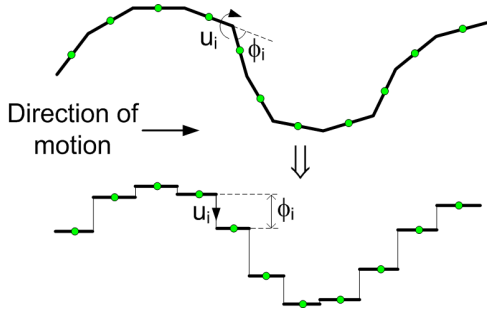

Fig. 1. The revolute joints of the snake robot are modelled as prismatic joints that displace the CM of each link transversal to the direction of motion.

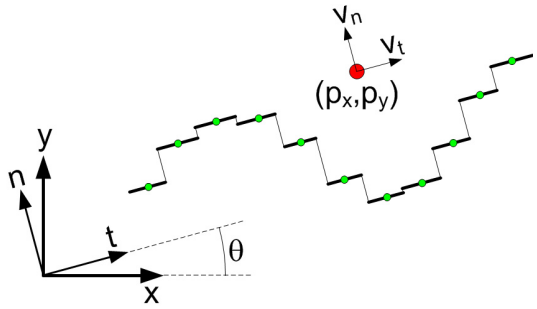

Fig. 2. Illustration of the two coordinate frames employed in the model. The global x-y frame is fixed. The t-n frame is always aligned with the snake robot.

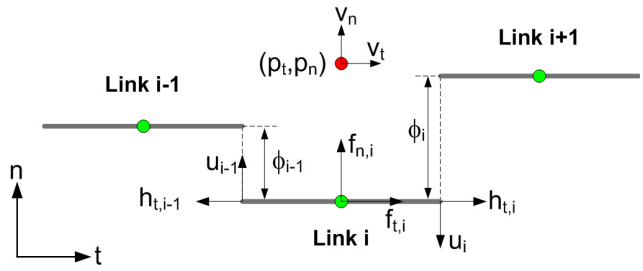

Fig. 3. Symbols characterizing the kinematics and dynamics of the snake robot.

A. Overview of the model

We consider a planar snake robot with links interconnected by active revolute joints. The surface beneath the robot is flat and horizontal, and each link is subjected to a viscous ground friction force. The body shape changes of the robot induce friction forces on the links, which subsequently produce translational and rotational motion of the robot. A simplified model that captures only the most essential part of the snake robot dynamics is proposed in [13]. The idea behind this model is illustrated in Fig. 1 and motivated by an analysis presented in [13], which shows that:

- The forward motion of a planar snake robot is produced by the link velocity components that are *normal* to the forward direction.
- The change in body shape during forward locomotion primarily consists of relative displacements of the CM of the links *normal* to the forward direction of motion.

Based on these two properties, the simplified model describes the body shape changes of a snake robot as *linear displacements* of the links with respect to each other instead of rotational displacements. The linear displacements occur *normal* to the forward direction of motion and produce friction forces that propel the robot forward. This essentially means that the revolute joints of the snake robot are modelled as prismatic (translational) joints and that the rotational motion of the links during body shape changes is disregarded. However, the model still captures the *effect* of the rotational link motion during body shape changes, which is a linear displacement of the CM of the links normal to the forward direction of motion.

A model of the snake robot is summarized in the following subsections in terms of the symbols illustrated in Fig. 2 and Fig. 3.

B. Kinematics of the snake robot

The snake robot has N links of length l and mass m interconnected by $N-1$ prismatic joints. The prismatic joints control the normal direction distance between the links. As seen in Fig. 3, the normal direction distance from link i to link $i+1$ is denoted by ϕ_i and represents the coordinate of joint i. The positive direction of ϕ_i is along the n axis.

The snake robot moves in the horizontal plane and has $N+2$ degrees of freedom. The motion is defined with respect to the two coordinate frames illustrated in Fig. 2. The x-y frame is the fixed global frame. The t-n frame is always aligned with the snake robot, i.e. the t and n axis always point in the *tangential* and *normal* direction of the robot, respectively. The origin of both frames are fixed and coincide.

As seen in Fig. 2 and Fig. 3, the global frame position of the CM (center of mass) of the snake robot is denoted by $(p_x, p_y) \in \mathbb{R}^2$, while the t-n frame position is denoted by $(p_t, p_n) \in \mathbb{R}^2$. The global frame orientation is denoted by $\theta \in \mathbb{R}$ and is expressed with respect to the global x axis with counterclockwise positive direction. The angle between the global x axis and the t axis is also θ since the t-n frame is always aligned with the snake robot. The relationship between the t-n frame and the global frame position is given by

$$p_t = p_x \cos\theta + p_y \sin\theta \tag{1}$$
$$p_n = -p_x \sin\theta + p_y \cos\theta \tag{2}$$

C. Equations of motion

The state vector of the model is chosen as

$$\boldsymbol{x} = (\boldsymbol{\phi}, \theta, p_t, p_n, \boldsymbol{v}_\phi, v_\theta, v_t, v_n) \in \mathbb{R}^{2N+4} \tag{3}$$

where $\boldsymbol{\phi} = (\phi_1, \cdots, \phi_{N-1}) \in \mathbb{R}^{N-1}$ are the joint coordinates, $\theta \in \mathbb{R}$ is the absolute orientation, $(p_t, p_n) \in \mathbb{R}^2$ is the t-n frame position of the CM, $\boldsymbol{v}_\phi = \dot{\boldsymbol{\phi}} \in \mathbb{R}^{N-1}$ are the joint velocities, $v_\theta = \dot{\theta} \in \mathbb{R}$ is the angular velocity, and $(v_t, v_n) \in \mathbb{R}^2$ is the tangential and normal direction velocity of the snake robot.

As illustrated in Fig. 3, each link is influenced by a ground friction force (acting on the CM of the link) and constraint

forces that hold the joints together. A model of these forces is presented in [13], where it is also shown that the complete model of the snake robot can be written as

$$\dot{\boldsymbol{\phi}} = \boldsymbol{v}_\phi \tag{4a}$$
$$\dot{\theta} = v_\theta \tag{4b}$$
$$\dot{p}_t = v_t + p_n v_\theta \tag{4c}$$
$$\dot{p}_n = v_n - p_t v_\theta \tag{4d}$$
$$\dot{\boldsymbol{v}}_\phi = -\frac{c_1}{m}\boldsymbol{v}_\phi + \frac{c_2}{m} v_t \boldsymbol{A}\boldsymbol{D}^T\boldsymbol{\phi} + \frac{1}{m}\boldsymbol{D}\boldsymbol{D}^T\boldsymbol{u} \tag{4e}$$
$$\dot{v}_\theta = -c_3 v_\theta + \frac{c_4}{N-1} v_t \overline{\boldsymbol{e}}^T\boldsymbol{\phi} \tag{4f}$$
$$\dot{v}_t = -\frac{c_1}{m}v_t + \frac{2c_2}{Nm} v_n \overline{\boldsymbol{e}}^T\boldsymbol{\phi} - \frac{c_2}{Nm}\boldsymbol{\phi}^T\boldsymbol{A}\overline{\boldsymbol{D}}\boldsymbol{v}_\phi \tag{4g}$$
$$\dot{v}_n = -\frac{c_1}{m}v_n + \frac{2c_2}{Nm} v_t \overline{\boldsymbol{e}}^T\boldsymbol{\phi} \tag{4h}$$

where $\boldsymbol{u} \in \mathbb{R}^{N-1}$ are the actuator forces at the joints and

$\overline{\boldsymbol{e}} = \begin{bmatrix} 1 & . & . & 1 \end{bmatrix}^T \in \mathbb{R}^{N-1}$,

$\overline{\boldsymbol{D}} = \boldsymbol{D}^T\left(\boldsymbol{D}\boldsymbol{D}^T\right)^{-1} \in \mathbb{R}^{N\times(N-1)}$,

$$\boldsymbol{A} = \begin{bmatrix} 1 & 1 & & \\ & . & . & \\ & & . & . \\ & & & 1 \quad 1 \end{bmatrix}, \boldsymbol{D} = \begin{bmatrix} 1 & -1 & & \\ & . & . & \\ & & . & . \\ & & & 1 \quad -1 \end{bmatrix},$$

where $\boldsymbol{A} \in \mathbb{R}^{(N-1)\times N}$ and $\boldsymbol{D} \in \mathbb{R}^{(N-1)\times N}$. The parameters c_1, c_2, c_3, and c_4 are scalar friction coefficients that characterize the external forces acting on the snake robot. More specifically, the coefficient c_1 determines the magnitude of the friction forces resisting the link motion, c_2 determines the magnitude of the induced friction forces that propel the snake robot forward, c_3 determines the friction torque opposing the rotation of the snake robot, while c_4 determines the induced torque that rotates the snake robot (this torque is induced when the forward direction velocity and the average of the joint coordinates are nonzero). The role of each coefficient is explained in more detail in [13].

We will assume that the actuator forces are always set according to the linearizing control law

$$\boldsymbol{u} = m\left(\boldsymbol{D}\boldsymbol{D}^T\right)^{-1}\left(\overline{\boldsymbol{u}} + \frac{c_1}{m}\dot{\boldsymbol{\phi}} - \frac{c_2}{m} v_t \boldsymbol{A}\boldsymbol{D}^T\boldsymbol{\phi}\right) \tag{5}$$

where $\overline{\boldsymbol{u}} \in \mathbb{R}^{N-1}$ is a new set of control inputs. This control law transforms the joint dynamics (4e) into $\dot{\boldsymbol{v}}_\phi = \overline{\boldsymbol{u}}$.

III. Stabilizability analysis of the snake robot

This section presents and proves a fundamental theorem concerning the properties of an asymptotically stabilizing control law for the snake robot to any equilibrium point $\boldsymbol{x}^e = (\boldsymbol{\phi}^e, \theta^e, p_t^e, p_n^e, \boldsymbol{v}_\phi = 0, v_\theta = 0, v_t = 0, v_n = 0)$. A well-known result by Brockett [14] states that a necessary condition for the existence of a *time-invariant* (i.e. not explicitly dependent on time) *continuous* state feedback law, $\boldsymbol{u} = \boldsymbol{u}(\boldsymbol{x})$, that makes $\boldsymbol{x}^e$ asymptotically stable, is that the image of the mapping $(\boldsymbol{x}, \boldsymbol{u}) \mapsto \dot{\boldsymbol{x}}$ contains some neighbourhood of $\dot{\boldsymbol{x}} = \boldsymbol{0}$. A result by Coron and Rosier [15] states that a control system that can be asymptotically stabilized (in the Filippov sense [15]) by a *time-invariant discontinuous* state feedback law can be asymptotically stabilized by a *time-varying continuous* state feedback law. If, moreover, the control system is *affine* (i.e. linear with respect to the control input), then it can be asymptotically stabilized by a *time-invariant continuous* state feedback law. We now employ these results to prove the following fundamental result:

Proposition 1: An asymptotically stabilizing feedback control law for a planar snake robot described by (4) to any equilibrium point must be time-varying, i.e. of the form $\boldsymbol{u} = \boldsymbol{u}(\boldsymbol{x}, t)$.

Proof: The result by Brockett [14] states that the mapping $(\boldsymbol{x}, \boldsymbol{u}) \mapsto \dot{\boldsymbol{x}}$ must map an arbitrary neighbourhood of $\boldsymbol{x}^e$ onto a neighbourhood of $\dot{\boldsymbol{x}} = \boldsymbol{0}$. For this to be true, points of the form $\dot{\boldsymbol{x}} = \left(\dot{\boldsymbol{\phi}} = \boldsymbol{0}, \dot{\theta} = 0, \dot{p}_t = 0, \dot{p}_n = 0, \dot{\boldsymbol{v}}_\phi = \boldsymbol{0}, \dot{v}_\theta = 0, \dot{v}_t = \epsilon, \dot{v}_n = 0\right)$ must be contained in this mapping for some arbitrary $\epsilon \neq 0$ because points of this form are contained in every neighbourhood of $\dot{\boldsymbol{x}} = \boldsymbol{0}$. However, these points do not exist for the model (4) because $\dot{v}_t = 0 \neq \epsilon$ when all the other derivatives of the state vector are zero. Hence, the snake robot *cannot* be asymptotically stabilized to $\boldsymbol{x}^e$ by a *time-invariant continuous* state feedback law. Moreover, since the model is affine and *cannot* be asymptotically stabilized by a *time-invariant continuous* state feedback law, the result by Coron and Rosier [15] proves that the system can neither be asymptotically stabilized by a *time-invariant discontinuous* state feedback law. We can therefore conclude that an asymptotically stabilizing control law for the snake robot to any equilibrium point must be time-varying, i.e. of the form $\boldsymbol{u} = \boldsymbol{u}(\boldsymbol{x}, t)$. ■

Remark 2: The authors have previously presented a similar stabilizability analysis of a snake robot modelled by a more complex model [9], which produced an identical result as in Proposition 1. This supports the conjecture that the simplified model employed in this paper captures the essential part of the dynamics of planar snake locomotion.

IV. Controllability analysis of the snake robot

This section presents a controllability analysis of the snake robot.

A. Controllability of the linearized system

We assume that the joint dynamics has been linearized by the control law (5) so that $\dot{\boldsymbol{v}}_\phi = \overline{\boldsymbol{u}}$. This enables us to rewrite the model of the snake robot (4) in the standard form of a control affine system as

$$\dot{\boldsymbol{x}} = \boldsymbol{f}(\boldsymbol{x}) + \sum_{j=1}^{N-1} \boldsymbol{g}_j \overline{\boldsymbol{u}}_j \tag{6}$$

where $\boldsymbol{f}(\boldsymbol{x})$ contains all the terms from (4) with $\overline{\boldsymbol{u}} = \boldsymbol{0}_{(N-1)\times 1}$, $\overline{\boldsymbol{u}}_j$ is the jth element of the control input vector $\overline{\boldsymbol{u}} \in \mathbb{R}^{N-1}$, and

$$\boldsymbol{g}_j = \begin{bmatrix} \boldsymbol{0}_{(N+2)\times 1} \\ \boldsymbol{e}_j \\ \boldsymbol{0}_{3\times 1} \end{bmatrix} \tag{7}$$

where $\boldsymbol{e}_j$ denotes the jth standard basis vector in $\mathbb{R}^{N-1}$ (the jth column of $\boldsymbol{I}_{N-1}$). The linearization of the model (6) about an equilibrium point $\boldsymbol{x}^e$ can be written as

$$\dot{\boldsymbol{z}} = \mathcal{A}\boldsymbol{z} + \mathcal{B}\overline{\boldsymbol{u}} \tag{8}$$

where $\boldsymbol{z} = \boldsymbol{x} - \boldsymbol{x}^e$, $\mathcal{A} = \frac{\partial \boldsymbol{f}(\boldsymbol{x})}{\partial \boldsymbol{x}}\Big|_{\boldsymbol{x}^e} \in \mathbb{R}^{(2N+4)\times(2N+4)}$, and $\mathcal{B} = \begin{bmatrix}\boldsymbol{g}_1 & \cdots & \boldsymbol{g}_{N-1}\end{bmatrix} \in \mathbb{R}^{(2N+4)\times(N-1)}$. The controllability matrix of the linearized system is given by $\boldsymbol{R} = \begin{bmatrix}\mathcal{B} & \mathcal{A}\mathcal{B} & \mathcal{A}^2\mathcal{B} & \mathcal{A}^{2N+3}\mathcal{B}\end{bmatrix}$ and does *not* have full rank since it can be verified that $\operatorname{rank}(\boldsymbol{R}) = 2N+1$. The linearized model of the snake robot is therefore not controllable since the *Kalman rank condition* [16] is not satisfied. To study the controllability of the snake robot, we must therefore consider nonlinear controllability concepts.

B. Controllability of the nonlinear system

In the following, we will investigate the controllability of the snake robot in terms of *strong accessibility* [16] and *small-time local controllability* (STLC) [17]. *Strong accessibility* means that the dimension of the space that the system can reach in *exactly* time T for any $T > 0$ is equal to the dimension of the state space. Accessibility does *not* imply controllability, but is a necessary (but not sufficient) condition for *small-time local controllability* (STLC). STLC is a stronger property than controllability and implies that the control input can steer the system in any direction in an arbitrarily small amount of time. For second-order systems, STLC is only possible from equilibrium states. Only sufficient (not necessary) conditions for STLC exist.

We assume that the snake robot consists of $N = 4$ links interconnected by $N-1 = 3$ joints. The model of this robot will have $2N + 4 = 12$ states. We argue that the following controllability results will also be valid for a snake robot with more links. In particular, a snake robot with $N > 4$ links can behave as a snake robot with $N = 4$ links by fixing $(N-4)$ joint coordinates at zero and allowing the remaining two joints to move. By calculating Lie brackets of the system vector fields in (6), we can construct the following *accessibility algebra* [16] of the system evaluated at an equilibrium point $\boldsymbol{x}^e$:

$$\boldsymbol{\Delta}(\boldsymbol{x}^e) = \begin{bmatrix}\boldsymbol{\Delta}_1 & \cdots & \boldsymbol{\Delta}_{15}\end{bmatrix}_{\boldsymbol{x}^e} \in \mathbb{R}^{12\times 15} \tag{9}$$

where

$\boldsymbol{\Delta}_1 = \boldsymbol{g}_1, \boldsymbol{\Delta}_2 = \boldsymbol{g}_2, \boldsymbol{\Delta}_3 = \boldsymbol{g}_3,$
$\boldsymbol{\Delta}_4 = [\boldsymbol{f}, \boldsymbol{g}_1], \boldsymbol{\Delta}_5 = [\boldsymbol{f}, \boldsymbol{g}_2], \boldsymbol{\Delta}_6 = [\boldsymbol{f}, \boldsymbol{g}_3],$
$\boldsymbol{\Delta}_7 = [\boldsymbol{f}, [\boldsymbol{f}, \boldsymbol{g}_1]], \boldsymbol{\Delta}_8 = [\boldsymbol{f}, [\boldsymbol{f}, [\boldsymbol{f}, \boldsymbol{g}_1]]],$
$\boldsymbol{\Delta}_9 = [\boldsymbol{f}, [\boldsymbol{f}, [\boldsymbol{f}, [\boldsymbol{f}, \boldsymbol{g}_1]]]],$
$\boldsymbol{\Delta}_{10} = [\boldsymbol{g}_1, [\boldsymbol{f}, [\boldsymbol{f}, \boldsymbol{g}_2]]],$
$\boldsymbol{\Delta}_{11} = [\boldsymbol{g}_1, [\boldsymbol{f}, [\boldsymbol{f}, [\boldsymbol{f}, \boldsymbol{g}_2]]]],$
$\boldsymbol{\Delta}_{12} = [\boldsymbol{g}_1, [\boldsymbol{f}, [\boldsymbol{f}, [\boldsymbol{f}, [\boldsymbol{f}, \boldsymbol{g}_2]]]]],$
$\boldsymbol{\Delta}_{13} = [\boldsymbol{g}_1, [\boldsymbol{f}, [\boldsymbol{f}, [\boldsymbol{f}, [\boldsymbol{f}, [\boldsymbol{f}, \boldsymbol{g}_2]]]]]],$
$\boldsymbol{\Delta}_{14} = [\boldsymbol{g}_1, [\boldsymbol{f}, [\boldsymbol{f}, [\boldsymbol{f}, [\boldsymbol{f}, [\boldsymbol{f}, \boldsymbol{g}_3]]]]]],$
$\boldsymbol{\Delta}_{15} = [\boldsymbol{g}_2, [\boldsymbol{f}, [\boldsymbol{f}, [\boldsymbol{f}, [\boldsymbol{f}, [\boldsymbol{f}, \boldsymbol{g}_3]]]]]].$

The accessibility algebra satisfies the following property:

Property 3: The accessibility algebra, $\boldsymbol{\Delta}(\boldsymbol{x}^e)$, has full rank ($\operatorname{rank}(\boldsymbol{\Delta}(\boldsymbol{x}^e)) = 12$) as long as the sum of the joint coordinates is nonzero, i.e. as long as $\overline{\boldsymbol{e}}^T\boldsymbol{\phi} \neq 0$.

Due to space constraints, we cannot present the expressions contained in each column of $\boldsymbol{\Delta}(\boldsymbol{x}^e)$. However, Property 3 can be shown to hold by employing a computer software for symbolic mathematics, such as *Matlab Symbolic Toolbox*. Note that we have included three more columns than rows in $\boldsymbol{\Delta}(\boldsymbol{x}^e)$ because different pairs of columns become linearly independent at certain configurations. Including three redundant columns ensures that $\boldsymbol{\Delta}(\boldsymbol{x}^e)$ does not drop rank at these configurations. We are now ready to state the following result:

Proposition 4: A planar snake robot described by (4) with $N = 4$ links is *locally strongly accessible* from any equilibrium point $\boldsymbol{x}^e$ satisfying $\overline{\boldsymbol{e}}^T\boldsymbol{\phi} \neq 0$.

Proof: The system is locally strongly accessible from $\boldsymbol{x}^e$ if the accessibility algebra of the system evaluated at $\boldsymbol{x}^e$ has full rank and does not contain the drift vector field $\boldsymbol{f}$ by itself (i.e. unbracketed) [16]. By Property 3, the snake robot satisfies these conditions as long as $\overline{\boldsymbol{e}}^T\boldsymbol{\phi} \neq 0$. This completes the proof. ■

We now show that the snake robot does *not* satisfy sufficient conditions for *small-time local controllability* (STLC). STLC requires that we classify the Lie brackets of the system vector fields in terms of *good* and *bad* brackets. A Lie bracket is said to be *bad* if it contains the drift vector field $\boldsymbol{f}$ an odd number of times and each control vector field $\boldsymbol{g}_j$ an even number of times (0 is even). This classification is motivated by the fact that a bad bracket *may* have directional constraints. E.g. the drift vector $\boldsymbol{f}$ is *bad* because it only allows motion in its positive direction. The snake robot is STLC from an equilibrium point $\boldsymbol{x}^e$ if it is accessible from $\boldsymbol{x}^e$ and all *bad* brackets of the system can be neutralized, i.e. written as linear combinations of *good* brackets of lower *θ-degree* [17] or lower *l-degree* [18]. The model of the snake robot satisfies the following property:

Property 5: The brackets $\boldsymbol{g}_j$, $[\boldsymbol{f}, \boldsymbol{g}_j]$, $[\boldsymbol{g}_j, [\boldsymbol{f}, \boldsymbol{g}_k]]$, $[\boldsymbol{g}_j, [\boldsymbol{f}, [\boldsymbol{f}, \boldsymbol{g}_k]]]$, $[[\boldsymbol{f}, \boldsymbol{g}_j], [\boldsymbol{f}, \boldsymbol{g}_k]]$, $[\boldsymbol{f}, [\boldsymbol{f}, \boldsymbol{g}_j]]$, $[\boldsymbol{f}, [\boldsymbol{f}, [\boldsymbol{f}, \boldsymbol{g}_j]]]$, $\cdots$, $[\boldsymbol{f}, [\cdots [\boldsymbol{f}, \boldsymbol{g}_j]] \cdots]$, where $j, k \in \{1, 2, 3\}$ and $j \neq k$, are all *good* brackets, but does *not* span the entire 12-dimensional state space.

Due to space constraints, we are again unable to present the expressions contained in the brackets in Property 5. However, the property can be shown to hold by employing a computer software for symbolic mathematics, such as *Matlab Symbolic Toolbox*. Property 5 enables us to state the following result:

Proposition 6: A planar snake robot described by (4) with $N = 4$ links does *not* satisfy the sufficient conditions for *small-time local controllability* (STLC) presented in [17] and [18].

Proof: The bracket $[\boldsymbol{g}_j, [\boldsymbol{f}, [\boldsymbol{f}, [\boldsymbol{f}, \boldsymbol{g}_j]]]]$ of the system, where $j \in \{1, 2, 3\}$, is a *bad* bracket. The only *good* brackets of lower θ-degree or lower l-degree that can neutralize this bad bracket are of the form $\boldsymbol{g}_j$, $[\boldsymbol{f}, \boldsymbol{g}_j]$, $[\boldsymbol{g}_j, [\boldsymbol{f}, \boldsymbol{g}_k]]$, $[\boldsymbol{g}_j, [\boldsymbol{f}, [\boldsymbol{f}, \boldsymbol{g}_k]]]$, $[[\boldsymbol{f}, \boldsymbol{g}_j], [\boldsymbol{f}, \boldsymbol{g}_k]]$, $[\boldsymbol{f}, [\boldsymbol{f}, \boldsymbol{g}_j]]$, $[\boldsymbol{f}, [\boldsymbol{f}, [\boldsymbol{f}, \boldsymbol{g}_j]]]$, $\cdots$, $[\boldsymbol{f}, [\cdots [\boldsymbol{f}, \boldsymbol{g}_j]] \cdots]$, where $j, k \in \{1, 2, 3\}$ and $j \neq k$. By Property 5, these brackets do *not* span the entire 12-dimensional state space. We therefore cannot express the bad bracket as a linear combination of good brackets of lower θ-degree or lower l-degree. Since there are bad brackets of the system that cannot be neutralized, the system does not satisfy the conditions for STLC given in [17] and [18]. ■

Remark 7: The authors have previously presented a similar controllability analysis of a snake robot with $N = 4$ links modelled by a more complex model [9]. This analysis produced an identical result concerning STLC, but showed

that the accessibility algebra of the system has full rank except for configurations where all joint coordinates are equal ($\phi_1 = \phi_2 = ... = \phi_{n-1}$), which will be the case when the snake robot is lying straight or forming an arc. According to Proposition 4, a configuration is singular when the sum of the relative linear link displacements is zero. Since this sum is zero for both straight and arc shaped snake robots with revolute joints, the singular configurations of the complex model considered in [9] are actually contained in the singular configurations stated in Proposition 4. This similarity supports the conjecture that the simplified model proposed in this paper captures the essential part of the dynamics of planar snake locomotion. Note anyhow that the most important conclusion to be drawn from Proposition 4 is that the snake robot is locally strongly accessible from *almost* any equilibrium point, except for certain singular configurations. This is in accordance with the result from [9].

V. Controller design

We will control the snake robot according to a motion pattern called *lateral undulation*, which consists of horizontal waves that are propagated backwards along the snake body from head to tail. As proposed in [2], lateral undulation is achieved by controlling joint $i \in \{1, \cdots, N-1\}$ of the snake robot according to the sinusoidal reference

$$\phi_{i,\mathrm{ref}} = \alpha \sin\left(\omega t + (i-1)\,\delta\right) + \phi_o \tag{10}$$

where α and ω are the amplitude and frequency, respectively, of the sinusoidal joint motion and δ determines the phase shift between the joints. The parameter ϕ_o is a joint offset coordinate used to control the direction of the locomotion. We assume that ϕ_o is a constant offset, so that

$$\dot{\phi}_{i,\mathrm{ref}} = \alpha\omega \cos\left(\omega t + (i-1)\,\delta\right) \tag{11}$$

$$\ddot{\phi}_{i,\mathrm{ref}} = -\alpha\omega^2 \sin\left(\omega t + (i-1)\,\delta\right) \tag{12}$$

We choose the control input $\overline{\boldsymbol{u}}$ of the snake robot as

$$\overline{\boldsymbol{u}} = \ddot{\boldsymbol{\phi}}_{\mathrm{ref}} + k_d\left(\dot{\boldsymbol{\phi}}_{\mathrm{ref}} - \dot{\boldsymbol{\phi}}\right) + k_p\left(\boldsymbol{\phi}_{\mathrm{ref}} - \boldsymbol{\phi}\right) \tag{13}$$

where k_p and k_d are positive scalar controller gains and $\boldsymbol{\phi}_{\mathrm{ref}} \in \mathbb{R}^{N-1}$ are the joint reference coordinates. The error dynamics of the joints is therefore given by

$$\left(\ddot{\boldsymbol{\phi}}_{\mathrm{ref}} - \ddot{\boldsymbol{\phi}}\right) + k_d\left(\dot{\boldsymbol{\phi}}_{\mathrm{ref}} - \dot{\boldsymbol{\phi}}\right) + k_p\left(\boldsymbol{\phi}_{\mathrm{ref}} - \boldsymbol{\phi}\right) = 0 \tag{14}$$

which is clearly *exponentially stable* [19].

VI. Stability analysis of snake locomotion based on averaging theory

In this section, *averaging theory* [20] is employed in order to study the velocity dynamics of the snake robot during lateral undulation. We employ averaging theory since we are primarily interested in the overall, i.e. average, speed and direction of the locomotion. The periodic fluctuations about the average trajectory of the snake is not of particular interest.

A. Introduction to averaging theory

Consider a system of the form

$$\dot{\boldsymbol{x}} = \varepsilon \boldsymbol{f}(t, \boldsymbol{x}) \tag{15}$$

where ε is a small positive parameter characterizing the magnitude of the perturbations of the system and $\boldsymbol{f}(t, \boldsymbol{x})$ is T-periodic, i.e. $\boldsymbol{f}(t+T, \boldsymbol{x}) = \boldsymbol{f}(t, \boldsymbol{x})$. A system that, in 'average', behaves similarly to the system in (15) is given by

$$\dot{\boldsymbol{x}} = \varepsilon \boldsymbol{f}_{av}(\boldsymbol{x}) \tag{16}$$

where

$$\boldsymbol{f}_{av}(\boldsymbol{x}) = \frac{1}{T}\int_0^T \boldsymbol{f}(\tau, \boldsymbol{x}) d\tau \tag{17}$$

Note that the above integral should be calculated by treating the elements of the state vector $\boldsymbol{x}$ as constants. The smallness requirement on ε ensures that $\boldsymbol{x}$ varies slowly with t relative to the periodic excitation of the system. The system response will thereby be determined predominantly by the average of the excitation. The following theorem follows directly from a more general theorem stated in [19] (Theorem 10.4):

Theorem 8: Let $\boldsymbol{f}(t, \boldsymbol{x})$ and its partial derivatives with respect to $\boldsymbol{x}$ be continuous and bounded for $(t, \boldsymbol{x}) \in [0, \infty) \times \mathbb{R}^n$. Suppose $\boldsymbol{f}$ is T-periodic in t for some $T > 0$ and ε is a positive parameter. Let $\boldsymbol{x}(t, \varepsilon)$ and $\boldsymbol{x}_{av}(t, \varepsilon)$ denote the solutions of (15) and (16), respectively. If the average system (16) has a *globally exponentially stable* equilibrium point and $\|\boldsymbol{x}(0, \varepsilon) - \boldsymbol{x}_{av}(0, \varepsilon)\| \leq k_0 \varepsilon$ for some $k_0 > 0$, then there exist $k > 0$ and $\varepsilon^* > 0$ such that for all $0 < \varepsilon < \varepsilon^*$,

$$\|\boldsymbol{x}(t, \varepsilon) - \boldsymbol{x}_{av}(t, \varepsilon)\| \leq k\varepsilon \quad \text{for all } t \in [0, \infty) \tag{18}$$

This theorem basically says that, for sufficiently small ε, the solutions of the original system (15) and the average system (16) remain close (of order ε) for all time if the initial conditions of the systems are close and the average system is *globally exponentially stable*.

B. Model of the velocity dynamics of the snake robot

We will now study the velocity dynamics of the snake robot during lateral undulation (the gait pattern defined in (10)). The velocity dynamics is defined by (4f), (4g), and (4h), which give the dynamics of the forward direction velocity v_t, the normal direction velocity v_n, and the angular velocity v_θ of the snake robot. It was shown in Section V that we can achieve exponentially stable tracking of the joint reference coordinates (10) with the control law (13). We will therefore assume that $\boldsymbol{\phi}$ and $\boldsymbol{v}_\phi = \dot{\boldsymbol{\phi}}$ are given by (10) and (11), respectively. Furthermore, in order to arrive at a model of the velocity dynamics which is in the standard averaging form (15), we assume that the amplitude α and frequency ω of the joint motion are always set according to the rule

$$\omega = \frac{k_{\alpha\omega}}{\alpha^2} \tag{19}$$

where $k_{\alpha\omega} > 0$ is a controller parameter. Note that α and ω are still independent parameters since any choice of α and ω can be obtained by choosing $k_{\alpha\omega} = \alpha^2\omega$. Using (10), (11), and (19), and introducing the velocity state vector $\boldsymbol{v} = (v_t, v_n, v_\theta) \in \mathbb{R}^3$, the velocity dynamics can be written as

$$\dot{\boldsymbol{v}} = \begin{bmatrix} \dot{v}_t \\ \dot{v}_n \\ \dot{v}_\theta \end{bmatrix} = \boldsymbol{f}(t, \boldsymbol{v}) \tag{20}$$

where

$$\boldsymbol{f}(t, \boldsymbol{v}) = \begin{bmatrix} -\frac{c_1}{m} v_t + \frac{2c_2}{Nm} v_n f_1(\omega t) - \frac{c_2}{Nm} f_2(\omega t) \\ -\frac{c_1}{m} v_n + \frac{2c_2}{Nm} v_t f_1(\omega t) \\ -c_3 v_\theta + \frac{c_4}{N-1} v_t f_1(\omega t) \end{bmatrix} \tag{21}$$

$$f_1(\omega t) = (N-1)\,\phi_o + \sum_{i=1}^{N-1} \alpha \sin\left(\omega t + (i-1)\,\delta\right) \tag{22}$$

$$\begin{aligned} f_2(\omega t) = \sum_{i=1}^{N-1} \sum_{j=1}^{N-1} \big[& \tfrac{k_{\alpha\omega}}{\alpha} \phi_o a_{ij} \cos\left(\omega t + (j-1)\,\delta\right) \\ & + k_{\alpha\omega} a_{ij} \sin\left(\omega t + (i-1)\,\delta\right) \cos\left(\omega t + (j-1)\,\delta\right) \big] \end{aligned} \tag{23}$$

and a_{ij} denotes element ij of the matrix $\boldsymbol{A}\overline{\boldsymbol{D}}$. To transform the model (20) into the standard form of averaging (15), we change the time scale from t to $\tau = \omega t$ and define $\varepsilon = 1/\omega$. Since $\frac{d}{dt} = \frac{1}{\varepsilon}\frac{d}{d\tau}$, the model (20) can now be written as

$$\frac{d\boldsymbol{v}}{d\tau} = \varepsilon \boldsymbol{f}(\tau, \boldsymbol{v}) \tag{24}$$

where

$$\boldsymbol{f}(\tau, \boldsymbol{v}) = \begin{bmatrix} -\frac{c_1}{m} v_t + \frac{2c_2}{Nm} v_n f_1(\tau) - \frac{c_2}{Nm} f_2(\tau) \\ -\frac{c_1}{m} v_n + \frac{2c_2}{Nm} v_t f_1(\tau) \\ -c_3 v_\theta + \frac{c_4}{N-1} v_t f_1(\tau) \end{bmatrix} \tag{25}$$

This model is in the standard form defined in (15). Note that when we require ε to be small, we equivalently require that $\omega = 1/\varepsilon$ is large.

C. Averaged model of the velocity dynamics

The averaged model of (24) is calculated in accordance with (16) as

$$\frac{d\boldsymbol{v}}{d\tau} = \varepsilon \frac{1}{2\pi} \int_0^{2\pi} \boldsymbol{f}(\tau, \boldsymbol{v}) d\tau \tag{26}$$

It can be verified that

$$\frac{1}{2\pi} \int_0^{2\pi} f_1(\tau) d\tau = (N-1)\,\phi_o \tag{27}$$

$$\frac{1}{2\pi} \int_0^{2\pi} f_2(\tau) d\tau = -\frac{1}{2} k_{\alpha\omega} k_\delta \tag{28}$$

where the constant $k_\delta \in \mathbb{R}$ is defined as

$$k_\delta = \sum_{i=1}^{N-1} \sum_{j=1}^{N-1} a_{ij} \sin\left((j-i)\,\delta\right) \tag{29}$$

The averaged model can therefore be written as

$$\frac{d\boldsymbol{v}}{d\tau} = \varepsilon \left(\boldsymbol{\mathcal{A}} \boldsymbol{v} + \boldsymbol{b}\right) \tag{30}$$

where

$$\boldsymbol{\mathcal{A}} = \boldsymbol{\mathcal{A}}(\phi_o) = \begin{bmatrix} -\frac{c_1}{m} & \frac{2(N-1)}{Nm} c_2 \phi_o & 0 \\ \frac{2(N-1)}{Nm} c_2 \phi_o & -\frac{c_1}{m} & 0 \\ c_4 \phi_o & 0 & -c_3 \end{bmatrix} \tag{31}$$

$$\boldsymbol{b} = \boldsymbol{b}(\alpha, \omega, \delta) = \begin{bmatrix} \frac{c_2}{2Nm} k_{\alpha\omega} k_\delta \\ 0 \\ 0 \end{bmatrix} \tag{32}$$

By changing time scale back to t using that $\frac{d}{d\tau} = \varepsilon \frac{d}{dt}$, the averaged model is given by

$$\dot{\boldsymbol{v}} = \boldsymbol{\mathcal{A}} \boldsymbol{v} + \boldsymbol{b} \tag{33}$$

We see that the averaged model of the velocity dynamics is a linear system characterized by the parameters of the joint reference coordinates, i.e. by α, ω, δ, and ϕ_o.

D. Stability analysis of the velocity dynamics

Before we determine the stability properties of the averaged model (33), we remove the constant offset term $\boldsymbol{b}$ with the coordinate transformation $\boldsymbol{z} = \boldsymbol{v} + \boldsymbol{\mathcal{A}}^{-1}\boldsymbol{b}$. This gives

$$\dot{\boldsymbol{z}} = \dot{\boldsymbol{v}} = \boldsymbol{\mathcal{A}}\left(\boldsymbol{z} - \boldsymbol{\mathcal{A}}^{-1}\boldsymbol{b}\right) + \boldsymbol{b} = \boldsymbol{\mathcal{A}}\boldsymbol{z} \tag{34}$$

Employing a computer software for symbolic mathematics, such as *Matlab Symbolic Toolbox*, the eigenvalues of $\boldsymbol{\mathcal{A}}$ are easily calculated as

$$\operatorname{eig}(\boldsymbol{\mathcal{A}}) = \begin{bmatrix} -\frac{c_1}{m} - \frac{2(N-1)}{Nm} c_2 \phi_o \\ -\frac{c_1}{m} + \frac{2(N-1)}{Nm} c_2 \phi_o \\ -c_3 \end{bmatrix} \tag{35}$$

The equilibrium point $\boldsymbol{z} = \boldsymbol{0}$ is *globally exponentially stable* if all eigenvalues of $\boldsymbol{\mathcal{A}}$ are negative [19], which is easily seen to be the case if

$$|\phi_o| < \frac{N}{2\,(N-1)} \frac{c_1}{c_2} \tag{36}$$

This is a limit on the amplitude of the joint coordinate offset ϕ_o, and is a function of the friction coefficients c_1 and c_2. It is not surprising that the model of the snake robot (4) can become unstable since the approach of modelling the link motion as translational displacements must naturally break down at some point. The instability issue in (36) is not relevant to a snake robot with revolute joints since the normal direction distance between the links of this mechanism will be physically constrained by the revolute joints.

Assuming that we choose ϕ_o to satisfy the limit (36), then $\boldsymbol{z}$ will converge exponentially to zero, which means that $\boldsymbol{v}$ will converge exponentially to $-\boldsymbol{\mathcal{A}}^{-1}\boldsymbol{b}$, which means that the average velocity will converge exponentially to the steady state velocity

$$\overline{\boldsymbol{v}} = -\boldsymbol{\mathcal{A}}^{-1}\boldsymbol{b} = \begin{bmatrix} \overline{v}_t & \overline{v}_n & \overline{v}_\theta \end{bmatrix}^T \tag{37}$$

which is given analytically by

$$\overline{v}_t = k_{\alpha\omega} k_\delta \frac{N c_1 c_2}{2\left(N^2 c_1^2 - (4N^2 - 8N + 4)\, c_2^2 \phi_o^2\right)} \tag{38a}$$

$$\overline{v}_n = k_{\alpha\omega} k_\delta \frac{\phi_o (N-1)\, c_2^2}{N^2 c_1^2 - (4N^2 - 8N + 4)\, c_2^2 \phi_o^2} \tag{38b}$$

$$\overline{v}_\theta = k_{\alpha\omega} k_\delta \frac{\phi_o N c_1 c_2 c_4}{2c_3\left(N^2 c_1^2 - (4N^2 - 8N + 4)\, c_2^2 \phi_o^2\right)} \tag{38c}$$

We can see that the resulting steady state velocity of the snake robot is proportional to the controller parameters $k_{\alpha\omega} = \alpha^2\omega$ and k_δ, and that the velocity also depends on nonlinear terms involving the joint coordinate offset ϕ_o. We can for example immediately see that the steady state velocity of the snake robot when it conducts lateral undulation with zero joint offset ($\phi_o = 0$) is given by $\overline{v}_t = \frac{c_2}{2Nc_1} k_{\alpha\omega} k_\delta$, $\overline{v}_n = 0$, and $\overline{v}_\theta = 0$.

Since the averaged model of the velocity dynamics given by (33) is *globally exponentially stable* (assuming that (36) is satisfied), it follows from Theorem 8 that, for sufficiently small ε (i.e. for sufficiently large ω), the average velocity given by (33) will approximate the exact velocity (20) for all time, and that the error of this approximation is of order ε, i.e. bounded in accordance with (18). In this paper, we will not investigate the lower limit of ω corresponding to some maximum error bound. However, the simulation results presented in Section VII shows that the exact and the average velocity agree well when ω is set to values that are commonly used for snake robot locomotion.

We now summarize the above conclusions.

Proposition 9: Consider a planar snake robot described by (4). Suppose the joint coordinates $\boldsymbol{\phi}$ are controlled in exact accordance with (10) and (11), and that the joint coordinate offset ϕ_o satisfies (36). Then there exist $k > 0$ and $\omega^* > 0$ such that for all $\omega > \omega^*$,

$$\|\boldsymbol{v}(t) - \boldsymbol{v}_{av}(t)\| \leq \tfrac{k}{\omega} \quad \text{for all } t \in [0, \infty) \tag{39}$$

where $\boldsymbol{v}(t)$ denotes the exact velocity of the snake robot given by (20) and $\boldsymbol{v}_{av}(t)$ denotes the average velocity given by (33). Furthermore, the average velocity $\boldsymbol{v}_{av}(t)$ of the snake robot will converge exponentially fast to the steady state velocity $\overline{\boldsymbol{v}}$ given by (37).

Remark 10: Proposition 9 is a powerful result. First of all, it proves mathematically that lateral undulation enables a wheel-less snake robot with anisotropic ground friction properties to achieve forward propulsion. To the authors' best knowledge, such a proof has never before been presented. Secondly, the result gives an analytical expression for the steady state velocity as a function of the controller parameters α, ω, δ, and ϕ_o, i.e. the amplitude, frequency, phase shift and offset of the joint motion during lateral undulation. This information is relevant for motion planning purposes. We can e.g. use the result to determine the phase shift δ that will maximize the forward velocity of the robot. A final powerful feature of the result is that it applies to snake robots with an arbitrary number of links N.

VII. Simulation Results

This section presents simulation results in order to investigate the validity of Proposition 9.

A. Simulation parameters

The exact model of the snake robot was given by (4) under the assumption that $\boldsymbol{\phi}$ was controlled in exact accordance with (10). The averaged model of the snake robot was given by (33). Both models were implemented and simulated in *Matlab R2008b* on a laptop running *Windows XP*. The dynamics was calculated using the *ode45* solver in Matlab with a relative and absolute error tolerance of 10^{-6}.

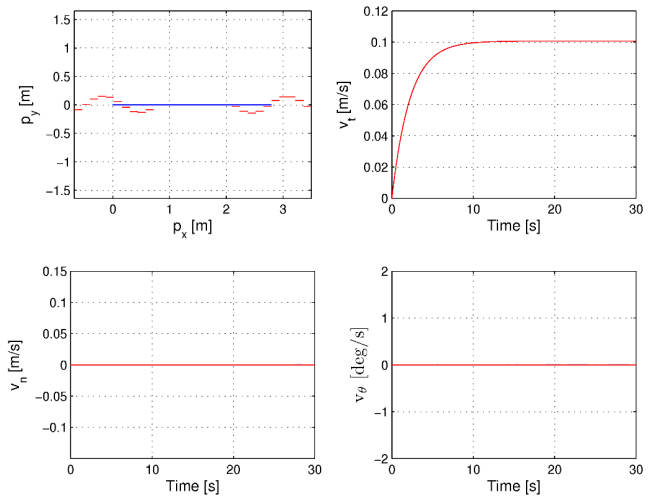

Fig. 4. Lateral undulation along a straight line with the controller parameters $\alpha = 0.1$ m, $\omega = 70°/\text{s}$, $\delta = 40°$, and $\phi_o = 0$ m. Both the exact (blue) and the average (red) velocities are plotted.

We assumed that the snake robot had $N = 10$ links of length $l = 0.14$ m and mass $m = 1$ kg. Furthermore, we chose the friction coefficients as $c_1 = 0.45$, $c_2 = 3$, $c_3 = 0.5$ and $c_4 = 20$, the initial state values as $(\boldsymbol{\phi}=\mathbf{0}, \theta=0, p_t=0, p_n=0, \boldsymbol{v}_\phi=\mathbf{0}, v_\theta=0, v_t=0, v_n=0)$, and the controller gains as $k_p = 20$ and $k_d = 5$. The values of the controller parameters α, ω, δ, and ϕ_o are presented with each simulation result.

B. Simulation results

The motion of the snake robot during lateral undulation was first simulated with the controller parameters $\alpha = 0.1$ m, $\omega = 70°/\text{s}$, $\delta = 40°$, and $\phi_o = 0$ m. Proposition 9 then states that the average velocity of the snake robot will converge exponentially fast to the steady state velocity $\overline{v}_t = \frac{c_2}{2Nc_1} k_{\alpha\omega} k_\delta \approx 0.10$ m/s, $\overline{v}_n = 0$ m/s, and $\overline{v}_\theta = 0°/\text{s}$. This is in agreement with the simulation result shown in Fig. 4. The top left plot illustrates the global CM position of the snake robot and the body shape at $t = 1$ s and $t = 30$ s. The other three plots show the exact and the average velocities of the snake robot. There is almost an exact overlap between the plots from the exact and the averaged model. This suggests that $\omega = 70°/\text{s}$ is well above the (unknown) value of ω^* described in Proposition 9.

In the next simulation, the controller parameters were set to $\alpha = 0.1$ m, $\omega = 70°/\text{s}$, $\delta = 40°$, and $\phi_o = l/8$ m. The joint coordinates were, in other words, offseted by $1/8$ of the link length l. In accordance with Proposition 9, the average velocity of the snake robot should then converge to $\overline{v}_t \approx 0.11$ m/s, $\overline{v}_n \approx 0.022$ m/s, and $\overline{v}_\theta \approx 4.23°/\text{s}$. This agrees very well with the simulation result shown in Fig. 5, which also shows a close overlap between the velocity plots from the exact and the averaged model.

In the final simulation, the controller parameters were set to $\alpha = 0.1$ m, $\omega = 30°/\text{s}$, $\delta = 40°$, and $\phi_o = -l/4$ m. The joint coordinates were, in other words, offseted by $1/4$ of the link length l. In addition, we reduced the frequency of the sinusoidal motion from $\omega = 70°/\text{s}$ to $\omega = 30°/\text{s}$ to

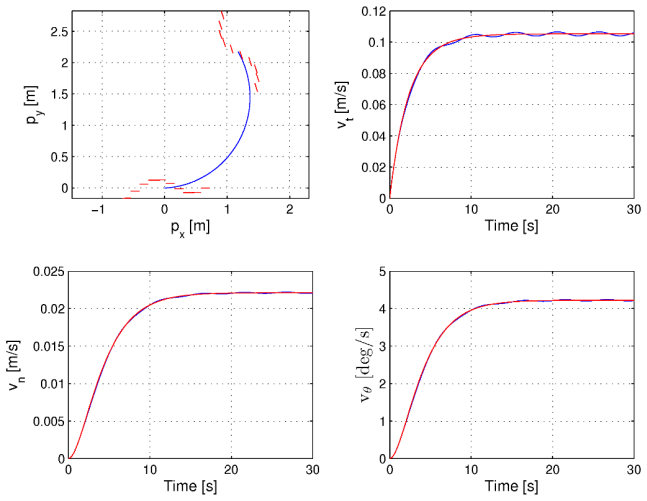

Fig. 5. Counterclockwise turning during lateral undulation with the controller parameters $\alpha = 0.1$ m, $\omega = 70°/s$, $\delta = 40°$, and $\phi_o = l/8$ m. Both the exact (blue) and the average (red) velocities are plotted.

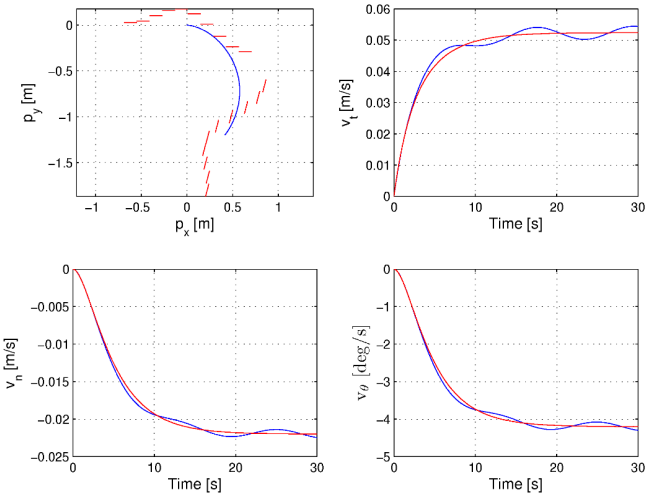

Fig. 6. Clockwise turning during lateral undulation with the controller parameters $\alpha = 0.1$ m, $\omega = 30°/s$, $\delta = 40°$, and $\phi_o = -l/4$ m. Both the exact (blue) and the average (red) velocities are plotted.

see how this affected the estimate of the average velocity. From Proposition 9, the average velocity should converge to $\overline{v}_t \approx 0.052$ m/s, $\overline{v}_n \approx -0.022$ m/s, and $\overline{v}_\theta \approx -4.20°/s$. This agrees very well with the simulation result shown in Fig. 6. The figure shows that there is still a good agreement between the velocities from the exact and the averaged model even though we reduced ω considerably.

VIII. Conclusions and Future Work

This paper has investigated the controllability and stability properties of a planar snake robot influenced by anisotropic viscous ground friction.

The paper has shown that any asymptotically stabilizing control law for the snake robot to an equilibrium point must be *time-varying*. Furthermore, it was shown that a snake robot (with four links) is *strongly accessible* from *almost* any equilibrium point, except for certain singular configurations, and that the robot does *not* satisfy sufficient conditions for *small-time local controllability* (STLC). The velocity dynamics of the snake robot during *lateral undulation* was investigated based on *averaging theory*. It was proven that the average velocity of the snake will converge exponentially fast to a steady state velocity, and an analytical expression for calculating the steady state velocity was given. In particular, explicit analytical relations between the steady state velocity and the amplitude, frequency, phase shift and offset of the joint motion during lateral undulation were given. In future work, the authors will employ the theoretical findings in this paper in order to develop and analyse motion planning strategies for snake robots.

References

[1] J. Gray, "The mechanism of locomotion in snakes," *J. Exp. Biol.*, vol. 23, no. 2, pp. 101–120, 1946.

[2] S. Hirose, *Biologically Inspired Robots: Snake-Like Locomotors and Manipulators*. Oxford: Oxford University Press, 1993.

[3] J. P. Ostrowski, "The mechanics and control of undulatory robotic locomotion," Ph.D. dissertation, California Institute of Technology, 1996.

[4] M. Saito, M. Fukaya, and T. Iwasaki, "Serpentine locomotion with robotic snakes," *IEEE Contr. Syst. Mag.*, vol. 22, no. 1, pp. 64–81, February 2002.

[5] G. P. Hicks, "Modeling and control of a snake-like serial-link structure," Ph.D. dissertation, North Carolina State University, 2003.

[6] M. Nilsson, "Serpentine locomotion on surfaces with uniform friction," in *Proc. IEEE/RSJ Int. Conf. Intelligent Robots and Systems*, 2004, pp. 1751–1755.

[7] A. A. Transeth, N. van de Wouw, A. Pavlov, J. P. Hespanha, and K. Y. Pettersen, "Tracking control for snake robot joints," in *Proc. IEEE/RSJ Int. Conf. Intelligent Robots and Systems*, San Diego, CA, USA, Oct-Nov 2007, pp. 3539–3546.

[8] J. Li and J. Shan, "Passivity control of underactuated snake-like robots," in *Proc. 7th World Congress on Intelligent Control and Automation*, June 2008, pp. 485–490.

[9] P. Liljebäck, K. Y. Pettersen, Ø. Stavdahl, and J. T. Gravdahl, "Controllability and stability analysis of planar snake robot locomotion," *IEEE Trans. Automatic Control*, 2010, conditionally accepted as Regular Paper.

[10] P. A. Vela, K. A. Morgansen, and J. W. Burdick, "Underwater locomotion from oscillatory shape deformations," in *Proc. IEEE Conf. Decision and Control*, vol. 2, Dec. 2002, pp. 2074–2080 vol.2.

[11] K. McIsaac and J. Ostrowski, "Motion planning for anguilliform locomotion," *IEEE Trans. Robot. Autom.*, vol. 19, no. 4, pp. 637–625, August 2003.

[12] K. Morgansen, B. Triplett, and D. Klein, "Geometric methods for modeling and control of free-swimming fin-actuated underwater vehicles," *IEEE Transactions on Robotics*, vol. 23, no. 6, pp. 1184–1199, Dec 2007.

[13] P. Liljebäck, K. Y. Pettersen, Ø. Stavdahl, and J. T. Gravdahl, "A simplified model of planar snake robot locomotion," in *Proc. IEEE/RSJ Int. Conf. Intelligent Robots and Systems*, 2010, accepted.

[14] R. Brockett, "Asymptotic stability and feedback stabilization," *Differential Geometric Control Theory*, pp. 181–191, 1983.

[15] J.-M. Coron and L. Rosier, "A relation between continuous time-varying and discontinuous feedback stabilization," *J. of Mathematical Systems, Estimation, and Control*, vol. 4, no. 1, pp. 67–84, 1994.

[16] H. Nijmeijer and A. v. d. Schaft, *Nonlinear Dynamical Control Systems*. New York: Springer-Verlag, 1990.

[17] H. J. Sussmann, "A general theorem on local controllability," *SIAM Journal on Control and Optimization*, vol. 25, no. 1, pp. 158–194, 1987.

[18] R. M. Bianchini and G. Stefani, "Graded approximations and controllability along a trajectory," *SIAM J. Control and Optimization*, vol. 28, no. 4, pp. 903–924, 1990.

[19] H. K. Khalil, *Nonlinear Systems*, 3rd ed. Prentice Hall, 2002.

[20] J. A. Sanders, F. Verhulst, and J. Murdock, *Averaging Methods in Nonlinear Dynamical Systems*, 2nd ed., ser. Applied Mathematical Sciences. Springer, 2007, vol. 59.